

X-ray Photoelectron Spectroscopy of CdSe Nanocrystals with Applications to Studies of the Nanocrystal Surface

J. E. Bowen Katari, V. L. Colvin, and A. P. Alivisatos*

Materials Science Division, Lawrence Berkeley Laboratory and Department of Chemistry,
University of California, Berkeley, California 94720

Received: December 13, 1993; In Final Form: February 10, 1994*

We report the use of X-ray photoelectron spectroscopy (XPS) to determine the surface composition of semiconductor nanocrystals. Crystalline, nearly monodisperse CdSe nanocrystals ranging in radius from 9 to 30 Å were chemically synthesized and covalently bound to Au and Si surfaces for study. XPS core level peak positions for Cd and Se were in agreement with those of bulk CdSe. We have determined that the majority of Se atoms on the surface are unbonded as prepared and that Cd atoms are bonded to the surface ligand, tri-*n*-octylphosphine oxide, to the extent that such bonding is sterically allowed. We have determined that the total ligand saturation of the nanocrystal surface varies from 60% in the smaller nanocrystals to 30% in the larger nanocrystals. In addition, we have determined that upon exposure of the nanocrystals to air Se surface sites are oxidized, forming a SeO₂ surface film which causes the nanocrystals to degrade over time. The nanocrystal surface can be modified by dispersing the crystals in pyridine. Nearly all of the P ligands are removed in this case, leaving behind primarily unsaturated Cd and Se surface atoms. In this case, both Cd and Se oxidize upon exposure to air.

Introduction

The surface of an inorganic nanocrystal plays an important role in determining its structural, thermodynamic, optical, and transport properties. Because of low symmetry and the absence of long-range order on the crystal surface, traditional probes of surface structure are not applicable. Thus, more is known about the interior composition and symmetry of nanocrystals than about the surface. In this paper we present a study of the surface composition of CdSe nanocrystals, with particular attention to the organic groups which cap the nanocrystals and to surface compounds formed after the nanocrystals are synthesized. This is in contrast to an XPS and Auger experiment which studied the composition of semiconductor nanocrystals onto which a layer of a different semiconductor had been grown.¹ In that work, the primary focus was on quantifying the relative amount of each type of semiconductor species and proving that a shell has actually been formed, rather than looking specifically at the outer surface layer.

Two previous experiments on the organic surface capping groups on cadmium chalcogenide nanocrystal surfaces have been performed.^{2,3} The first experiment used NMR to determine bonding geometry and surface coverage of thiophenol on CdS nanocrystals.² The second used ³¹P NMR to study the surface coverage of tri-*n*-octylphosphine oxide (TOPO) and TOPSe on CdSe nanocrystals.³ This more recent study determined the total coverage of P-containing ligands and determined the relative amount of TOPO vs TOPSe on the surface for 18-Å nanocrystals. NMR is probably the most powerful probe available for study of the bonding geometry at the nanocrystal surface. However, it does not immediately provide a route to the full composition of the surface. X-ray photoelectron spectroscopy provides such a probe of composition.

Recently, techniques were developed which allow the chemical binding of nanocrystals to Au and Al surfaces.⁴ The binding molecule situates the nanocrystals ~10 Å from the metal surface, allowing for electron tunneling between the nanocrystals and the surfaces in order to avoid charging. In addition, the samples are supported on a macroscopic surface. This has allowed the exploration of the range of more traditional surface techniques

for use on nanocrystals. In this paper we report the use of a traditional surface science technique, XPS, to explore the surface properties of semiconductor nanocrystals. We have synthesized nearly monodisperse, crystalline CdSe nanocrystals for this study, using a variation of a technique developed by Murray et al.⁵ We have bound the nanocrystals to Au and Si surfaces. Finally, we have performed XPS on a variety of CdSe nanocrystal sizes and determined the types of surface species present as well as the percent coverage of these species.

Experiment

Synthesis. Murray et al.⁵ have recently reported a powerful new method for making crystalline, monodisperse, size-tunable CdSe nanocrystals. We have adapted their method, with some changes that are reported below. The principal difference between the preparations is the temperature of injection, which affects the time evolution of the nanocrystal growth as well as the crystallinity and shape of the nanocrystals. The nanocrystals produced by the method below are nearly monodisperse without size-selective precipitation, are crystalline, and are spherical.

All of the following procedures are carried out using standard airless techniques. Dimethylcadmium was purchased from Strem Scientific and filtered prior to use. Se (60 mesh) powder, 99% tri-*n*-octylphosphine oxide (TOPO), tributylphosphine (TBP), and anhydrous methanol were used as received from Aldrich. Toluene (Aldrich) was distilled over sodium metal. Anhydrous pyridine was used as received from Burdick and Jackson.

A typical preparation proceeds as follows. A 0.8-g sample of Se is dissolved in 8.0 g of TBP, and 2.0 g of dimethylcadmium is then added. This solution is then diluted by 4:1 with TBP, and the resulting solution is septa capped and removed from the drybox. Twelve grams of TOPO is heated to ~350 °C under Ar. **WARNING:** Heating should be done with extreme caution as 350 °C is well above TOPO's flash point. Differences in temperature of less than 1 °C can change both the average size and the quality of the size distribution. When the temperature has stabilized, 0.4 mL of the Me₂Cd/Se solution is added. The solution immediately changes color, indicating the formation of nanocrystals. This solution is removed from the heat and allowed to cool. In order to prevent any oxidation of the nanocrystal surface, the solution is cooled to room temperature under Ar.

* Abstract published in *Advance ACS Abstracts*, March 15, 1994.

This solid solution is then transferred to the drybox where methanol is added, dissolving the TOPO and precipitating the nanocrystals. This mixture is then filtered through a 0.1- μm filter, and the recovered powder of nanocrystals is stored under nitrogen. In practice, little oxidation is observed when the precipitation and filtration are done in air, as long as the resulting powder is stored under nitrogen. The resulting nanocrystals can be dispersed in toluene and can also be dispersed in pyridine. Simply dispersing the nanocrystals in pyridine, without significant washing, is sufficient to change their surface composition. Note that we have used TBP as the Se solvent rather than trioctylphosphine (TOP), which is used by Murray et al.⁵ We initially used TBP in order to achieve low coverage of the Se surface atoms, as the tributylphosphine will more readily be removed in the high-temperature conditions that we use. However, comparison of our surface experiments with those of Becerra et al.³ indicates that the surface characteristics of nanocrystals synthesized using TOP and TBP are rather similar.

In order to make nanocrystals with absorption maxima larger than 580 nm, modifications of the above procedure are employed. One method is to cool the 350 °C solution to 320 °C and allow it to continue heating for several minutes. The size can be monitored by removing aliquots of the solution at time intervals. This does create larger nanocrystals; however, the initial size distribution is lost. A better way to increase the average size of the nanocrystals is to add stock solution in 0.1-mL intervals to a 300 °C solution over a period of several minutes. This technique allows for better retention of the initial size distribution than the pure heating method.

Characterization of Nanocrystals. Absorption spectra were obtained using an HP Model 8452 ultraviolet-visible absorption (UV-vis) diode array spectrometer with a collimated deuterium lamp source. The resolution is 2 nm. Samples were dispersed in toluene or pyridine for measurement. These solvents limit the useful lower limit of the spectrometer to ~ 320 nm.

Representative samples were characterized by X-ray powder diffraction using a Siemens Model D5000 X-ray diffractometer with Cu K α radiation. CdSe powders were placed on glass plates for measurement or were pressed onto Ta foils. The diffraction from most metal foils interferes with the CdSe pattern. However, Ta's crystal structure is such that it does not interfere. Domain sizes of nanocrystals were obtained by fitting the width of the peaks and translating this to domain sizes using standard formulas for spherical nanocrystals.⁶

Fourier transform infrared spectroscopy was performed using a Nicolet FTIR spectrometer. Powdered nanocrystal samples were mixed with KBr. The resulting powder was finely ground and pressed into an optically clear pellet using a hydraulic press. Spectra were collected over the range from 400 to 4000 cm^{-1} .

Sizing. Sizes of the nanocrystals were obtained by comparing optical absorption spectra of all samples to spectra from a large number of samples sized using transmission electron microscopy (TEM) and small-angle X-ray scattering (SAXS).⁷

Binding Nanocrystals to Surfaces. In order to perform photoelectron spectroscopy on the nanocrystals, the nanocrystals must first be attached to a conducting surface so that they will not charge during performance of the experiment. Several things are important for this attachment. First, the nanocrystals must be positioned a uniform distance from the conducting surface, and this distance must be very small. In addition, the nanocrystals must be in a single layer, with no nanocrystals sitting on top of other nanocrystals. Finally, the samples must be robust to facilitate transfer between different experiments. These three requirements are best satisfied by chemically binding the nanocrystals to the surface. Most of the samples used in this study were bound to gold surfaces using techniques described elsewhere.⁴ Briefly, hexanedithiol is allowed to self-assemble on ion-etched gold evaporated onto glass slides. The slides are then transferred to a solution of nanocrystals, which covalently bond to the sulfur of the hexanedithiol (Figure 1). Empirically, we

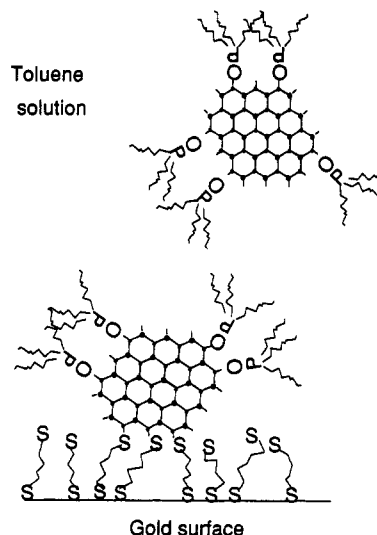


Figure 1. Attachment of CdSe nanocrystals dissolved in toluene to Au surfaces with hexanedithiol.

have found that hexanedithiol maximizes the nanocrystal coverage relative to longer and shorter chain dithiols. We believe that the longer chains can loop, forming two linkages to gold, while the shorter chains do not bind strongly enough to the gold to strongly bind the nanocrystals to the surface. Hexanedithiol most likely does not form an ordered monolayer, because of its length.⁸ However, it is possible to use a more complex method of binding, modeled after a method used on trichlorosilanes by Wasserman et al.,⁹ which should yield an ordered organic substrate to which to bind the nanocrystals. In this scheme, a long-chain alkanethiol with a terminating thioacetate group would be bound to the Au. After assembly, the thioacetate group could be converted to a thiol and exposed to the nanocrystals.

We have also bound nanocrystals to doped Si surfaces. p-doped Si(111) wafers were first cleaned by immersion in a 1:1 solution of methanol (Aldrich) and 45% hydrochloric acid (Aldrich), followed by immersion in concentrated sulfuric acid (Aldrich).¹⁰ The wafers were then rinsed with distilled water. The technique used to bind the nanocrystals to the cleaned and oxidized Si surface follows a technique used to bind Au coats to glass slides.¹¹ The wafers were placed in a boiling solution of 10 g of distilled water and 10 g of (3-mercaptopropyl)trimethoxysilane (MPS) (Sigma) in 400 g of 2-propanol (electronic grade, Aldrich). After 10 min, the wafers were removed, rinsed in 2-propanol, dried with Ar, and placed in a 100 °C oven. This was repeated three times. The wafers were then placed in a solution of CdSe nanocrystals and allowed to sit overnight. The wafers were then removed from solution and rinsed with the nanocrystals' solvent, dried with nitrogen, and stored. Note that for both techniques the MPS or hexanedithiol coated surfaces could be pumped into the glovebox, where the particle solution could be added without exposure to air. In practice, this was not necessary to avoid oxidation as long as the finished samples were stored under nitrogen.

Characterization on Surfaces. Resonance Raman spectroscopy was performed on the nanocrystals using a setup described previously.¹² Briefly, an Ar-ion pumped dye laser is used to excite the nanocrystals on resonance. The Raman scattering is then detected off axis using a double monochromator with output fed to a CCD camera. The samples were cooled to 77 K or lower under vacuum for the measurement, in order to allow accurate comparison with more traditional Raman experiments, which are done on polymer films at these temperatures.

Rutherford backscattering spectroscopy (RBS) provides a measure of the absolute number of atoms of each element per square centimeter on the sample surfaces, which can be translated to percent monolayer coverage. RBS was performed at the RBS facility of the Materials Science Division of Lawrence Berkeley Laboratory.

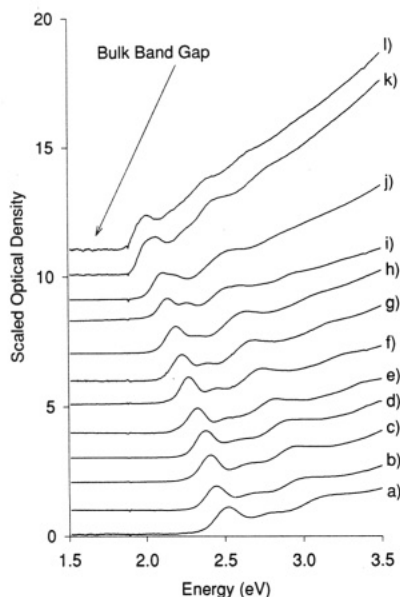


Figure 2. UV-vis absorption spectra of CdSe nanocrystals: (a) $r = 9.3$ Å; (b) $r = 10.0$ Å; (c) $r = 10.4$ Å; (d) $r = 10.7$ Å; (e) $r = 11.4$ Å; (f) $r = 12.3$ Å; (g) $r = 13.2$ Å; (h) $r = 14.1$ Å; (i) $r = 15.9$ Å; (j) $r = 18.0$ Å; (k) $r = 24.2$ Å; (l) $r = 33.5$ Å.

XPS was performed using a Perkin-Elmer PHI 5300 ESCA System machine located in the Materials Science Division of Lawrence Berkeley Laboratory. Both Mg and Al anodes driven at 400 W were used for this study. All scans were obtained using the 1-cm² aperture. Survey scans were collected over the range from 1100 to 0 eV with 179-eV pass energy detection, corresponding to a resolution of 4.5 eV. Typical surveys were collected for 5 min. Close-up scans were collected over a range of 20 eV around the peak of interest with either 8.9-eV pass energy detection or 35.7-eV pass energy detection, which correspond to 0.69- and 1.1-eV resolution, respectively, with the Mg anode. Typical close-up scans were detected for 10–20 min per element. Measurements were performed at pressures lower than 1×10^{-8} Torr. All spectra were calibrated using the position of the Au 4f peaks present in all spectra as a standard.

Results

Characterization of Samples. All samples were characterized using UV-vis. Spectra (Figure 2) indicate nearly monodisperse nanocrystals with a range in exciton peak position from 1.9 to 2.5 eV. The room temperature bulk band gap for wurtzite CdSe is 1.74 eV.¹³

X-ray diffraction patterns on a large number of samples indicate wurtzite nanocrystals.¹⁴ The domain sizes for the large majority of nanocrystals agreed with the sizing obtained by direct means, indicating good crystallinity of the nanocrystals. In addition, the shape of the spectra indicate spherical particles with few or no stacking faults, based on comparison to the calculated spectra of Murray et al.^{5,14}

TEM images of nanocrystals indicated good crystallinity of the nanocrystals and a spherical shape (Figure 3), justifying the straightforward treatment of the X-ray diffraction data. Sizes and distributions obtained from SAXS generally agreed with the TEM measurements, with the sizes from SAXS generally larger, because of the greater sensitivity to the disordered surface of SAXS.⁷ The curve used to size the nanocrystals is shown in Figure 4.

FTIR was used as a probe of the presence of TOPO on the nanocrystal surface. The nanocrystal spectrum had peaks matching all of the TOPO peaks in frequency and relative intensity, except for the P–O stretch, which was shifted lower by ~ 20 cm⁻¹ relative to bulk TOPO (Figure 5). This is in agreement with IR measurements performed on triphenylphosphine oxides

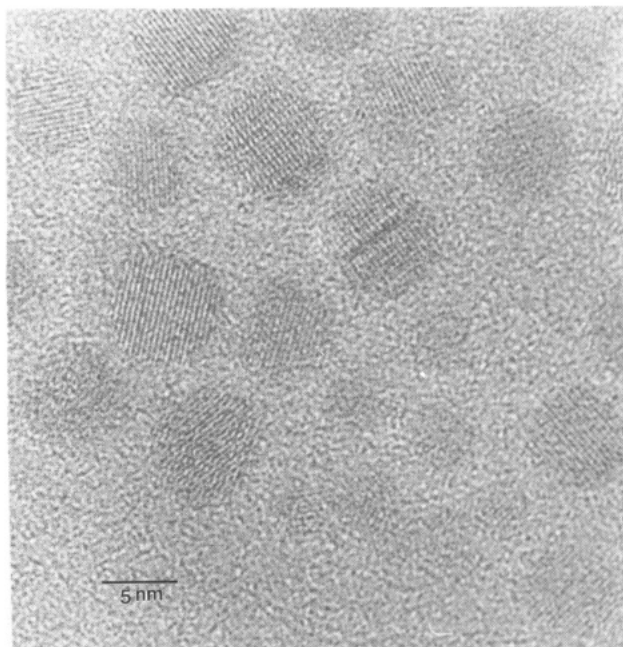


Figure 3. Transmission electron micrograph of CdSe nanocrystals.

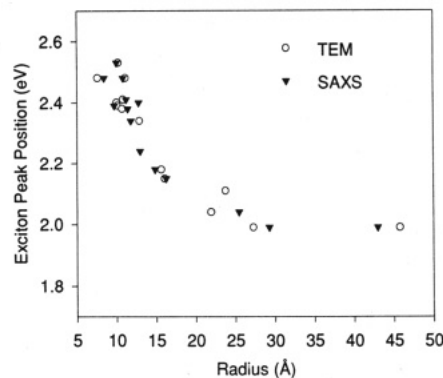


Figure 4. Exciton peak position from UV-vis vs measured radius from TEM and SAXS.

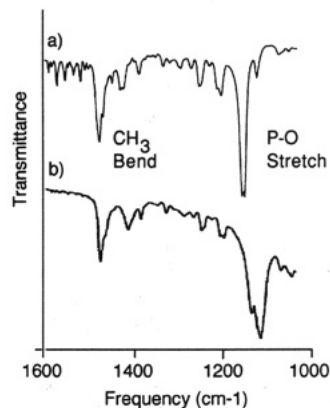


Figure 5. FTIR spectra: (a) TOPO dispersed in KBr; (b) CdSe nanocrystals dispersed in KBr.

complexing to CdI₂ and other metal salts,¹⁵ which typically show shifts in P–O frequency of between 20 and 60 cm⁻¹ upon complexation.

Raman spectroscopy (Figure 6) was used to confirm the presence of nanocrystals on the surface. Use of the Si substrate provides the built-in standard of the Si TO mode at 522 cm⁻¹. All samples show the presence of the CdSe LO mode at 212 cm⁻¹ as well as the first and second overtone. The presence of the surface quenches part of the fluorescence, allowing for greater ease of measurement of the spectrum of samples bound to surfaces than of samples in polymers or as powder. The Raman line width

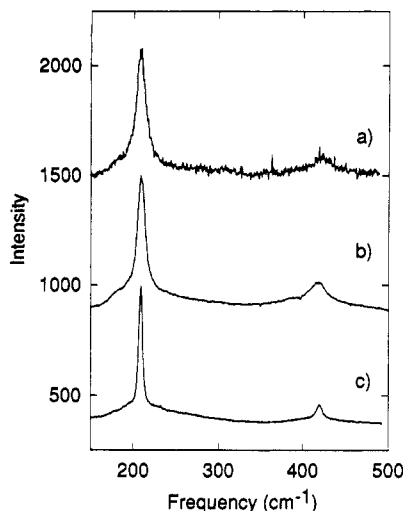


Figure 6. (a) Raman spectrum of CdSe nanocrystals bound to Si, taken at 77 K. $r = 9.3$ Å. (b, c) Raman spectra of CdSe nanocrystals bound to gold, taken at 16 K: (b) $r = 11.4$ Å; (c) $r = 18.0$ Å. Note that fluorescence has been quenched by the presence of the surfaces.

for the nanocrystals varies with size in the same way as in previous studies on CdS.^{12,16}

RBS measurements indicate coverage of $\sim 10^{15}$ Cd and Se atoms per cm^2 , which corresponds to $\sim 1/6$ of a monolayer of nanocrystals on the Si surface. The signal from the Au in RBS prevents use of the technique for gold substrate samples. However, comparison of the XPS signals from both types of samples indicates that coverage does not differ significantly between the two types of samples.

Together, these techniques indicate that nearly monodisperse and highly crystalline CdSe nanocrystals of wurtzite structure are present in $\sim 1/6$ monolayer coverage on Au and Si substrates. Because CdSe fails to show up in samples in which the hexanedithiol or MPS is not applied, these techniques also indicate that the samples are bound to the surfaces by the hexanedithiol or MPS. However, the degree of order of the dithiol and MPS is not assessed by these techniques and is expected to be low.

Determination of Composition from Photoelectron Spectra. In order to use an observed photoelectron spectrum to derive composition information, several factors must be accounted for. This is well described in Wagner et al.'s XPS handbook.¹⁷ In summary, the intensity of a peak (the relative number of electrons detected) in XPS from a single element for a homogeneous sample is

$$I = n f \sigma \theta y \lambda A T \quad (1)$$

where n is the number of atoms per cm^3 , f is the X-ray flux, σ is the cross section for the photoelectric process, θ is an angular factor, y is the efficiency for formation of photoelectrons with the full kinetic energy, λ is the escape depth of photoelectrons of that kinetic energy, A is the area of the sample being probed, and T is a factor for the efficiency of detecting electrons of a given kinetic energy. Inverting eq 1, we determine that

$$n = 1 / (f \sigma \theta y \lambda A T) \quad (2)$$

Typically, the entire denominator is bundled and called S , the atomic sensitivity factor. Values for this factor have been experimentally determined and theoretically calculated for a variety of different types of XPS systems.¹⁸ The numeric value will vary from system to system because the transmission factor will vary between different electron detection systems. In order to determine relative concentrations of atoms in a homogeneous system, one simply divides each atom's peak intensity by its sensitivity factor and takes the ratio.

In a nanocrystal sample, as in other types of heterogeneous systems, this straightforward analysis is not adequate because

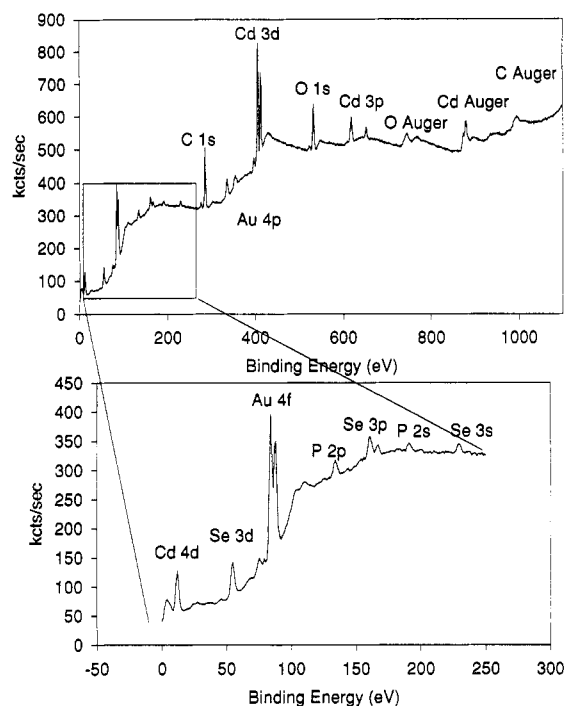


Figure 7. Typical XPS survey spectra of CdSe nanocrystals bound to gold using Mg X-ray source.

the equation assumes a homogeneous, thick (>200 nm) sample. This is manifested in the inclusion of λ as the factor for the escape depth. The appropriate way to account for the escape depth is to integrate over the entire region of interest, modifying the intensity from each point by an exponential factor which decreases with depth away from the surface.¹⁹ Thus, for a flat homogeneous sample, the appropriate integral is just

$$\int_0^d e^{-z/\lambda} dz \quad (3)$$

where d is the depth of the sample. Escape depths are in the range from 4 to 20 Å, so for $d > 20$ nm the integral is just equal to λ . However, in nanocrystals, the depth of the sample is of the same order of magnitude as the escape depth, and so the above equation will not hold. Now we must integrate the above equation over a sphere, with z modified to be the distance from a point within a sphere to the sphere's surface in the direction of the analyzer. Thus, in the calculation of the compositional ratios, the calculated sensitivity factors are divided by λ and then multiplied by the appropriate integral, and then the two factors are ratioed. Escape depths are ~ 15 Å for the Cd 3d cores, ~ 20 Å for the P 2p cores, and ~ 21 Å for the Se 3d cores for Mg $K\alpha$ radiation. In the end, the ratio of the two integrals is much closer to unity than the ratio of the two escape depths, because the nanocrystals are about the same size as the escape depths. The corrections performed in this way will alter the composition by as much as 30% in the smaller nanocrystals. This effect only becomes negligible ($<1\%$ difference) for diameters greater than ~ 90 Å.

Multiple XPS measurements have been taken on 22 different preparations of CdSe nanocrystals ranging in radius from 9.3 to 30.2 Å. Typical survey spectra (Figure 7) were obtained in 5 min using 178-eV pass energy. They show the presence of Au from the substrate, Cd, Se, and P from the nanocrystals and their surfaces, and C and O from the nanocrystals' surfaces and from absorbed gaseous molecules. The survey spectra give a rough idea of the coverage of nanocrystals on the surface—when the Cd 3d signal is larger than that from Au 4f, the coverage is comparable to Si substrate samples which had coverages of $\sim 1/6$ monolayer.

Higher-resolution spectra were taken of the Cd and Se regions of samples as prepared (Figure 8). The scans showed no evidence

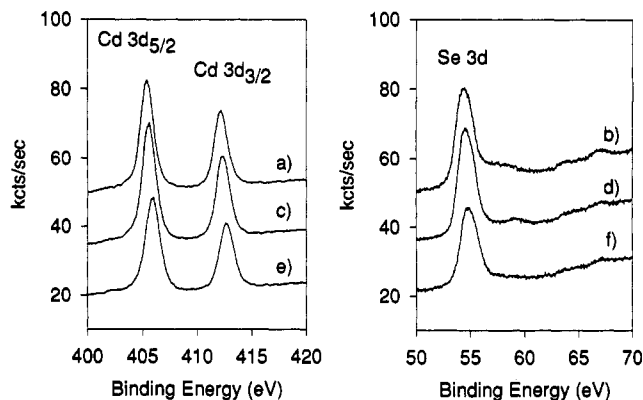


Figure 8. Close-up surveys for Cd 3d and Se 3d cores. Signals have been offset relative to each other for clarity. (a, b) $r = 10.0$ Å; (c, d) $r = 15.9$ Å; (e, f) $r = 12.3$ Å.

of peaks other than the Cd and Se cores from the main and satellite Mg X-rays, and the satellite peaks of Au, in the Se case. There was no evidence of shake-up peaks, which are photoemission peaks from species ionized prior to the observed photoemission process and generally occur several electronvolts to higher binding energy of the main peak in the spectra. Cd $3d_{5/2}$ peak positions ranged from 405.1 to 406.0 eV, with a normal distribution centered around 405.6 ± 0.2 eV. Se 3d peak positions ranged from 54.3 to 54.9 eV, with a normal distribution centered around 54.6 ± 0.2 eV. The Cd and Se peak positions moved together, so that the difference between the two peak positions averaged 351.0 ± 0.1 eV. In bulk CdSe, this difference is 350.97^{20} . Note that comparison of absolute positions is meaningless because the bulk studies are referenced to the valence band edge of CdSe, which we cannot see in our spectra due to the interference from the Au valence band. In addition, we would expect the valence band edge of our material to shift as a function of size, as in CdS,²¹ which also prevents comparison.

Peak areas of the Cd and Se cores were measured and used to calculate Cd to Se ratios for the nanocrystals as described above. Areas were determined by fitting each of the curves using a nonlinear least-squares curve-fitting program²² and taking the area of the fit peak. The absolute areas are only accurate to an error of $\sim 10\%$, because of the uncertainty in the precise shape of the background. However, the background is kept the same for all fits, and so the relative error is much smaller—the typical error in fits was 1–2%. An empirical correction was made for the pass energy variation between the two scans when there was a difference. The calculated Cd:Se ratio was 1.02 ± 0.14 and did not vary systematically with size. This average ratio is in agreement with elemental analysis of the powder samples. Deviations of composition measured by XPS from that determined by independent elemental analysis would indicate orientation of faceted nanocrystals upon binding to the gold surface. We have seen no evidence of this occurring.

Surface Properties of Nanocrystals Deposited from Toluene.

High-resolution scans of the P region of the nanocrystals deposited from toluene solution provide information about the surface of the nanocrystals. The P peak position is 133.7 ± 0.3 . This peak position is ~ 1.5 eV higher than the peak position for tertiary phosphine oxides, sulfides,¹⁷ and, by analogy, selenides. However, the IR shift of the P–O frequency to lower energy upon complexation indicates a transfer of electron density from P to the O, causing the P to be more positive when complexed to Cd¹⁵ and hence have larger binding energy. Experiments on P–metal bonds have been limited to studies of covalent bonds;¹⁷ however, an estimate of the binding energy of P in a tertiary phosphine datively bound to Cd can be made as follows. The binding energy of phosphorus in a tertiary phosphine is 129 eV.¹⁷ The binding energy of P in a tertiary phosphine oxide is 132 eV.¹⁷ Relative to the tertiary phosphine, P will be more positive when bound to Cd, as it will donate electrons to Cd, and thus its binding energy

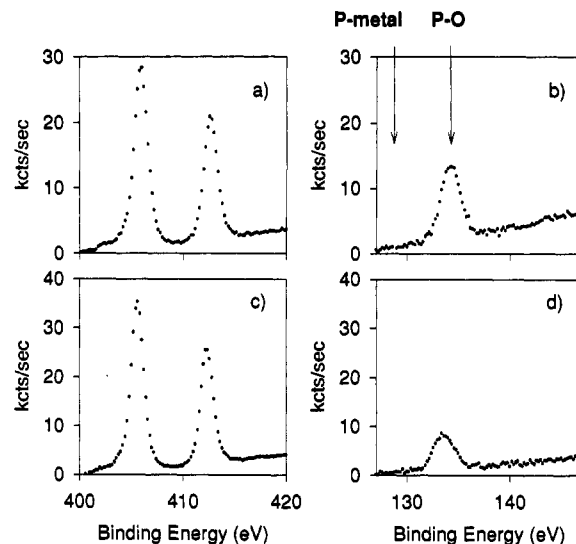


Figure 9. Close-up surveys for Cd 3d and P 2p cores. Signals have been corrected for the relative sensitivity factors. (a, b) $r = 10.0$ Å; (c, d) $r = 15.9$ Å. Note that the P/Cd ratio is smaller for the larger size.

TABLE 1

radius (Å)	P/Cd ratio	radius (Å)	P/Cd ratio	radius (Å)	P/Cd ratio
9.3	0.77	10.4	0.56	13.1	0.36
9.6	0.69	10.7	0.53	13.2	0.47
9.6	0.66	11.4	0.56	13.2	0.44
10.0	0.73	11.4	0.46	13.2	0.46
10.0	0.74	11.4	0.41	15.9	0.42
10.0	0.72	11.4	0.49	17.8	0.21
10.0	0.68	11.7	0.46	19.9	0.24
10.0	0.82	12.3	0.47	22.1	0.22
10.4	0.61	12.3	0.40	30.2	0.21

will be larger. Relative to a tertiary phosphine oxide, P will be less positive when bound to Cd, as it will not donate as much electron density to the Cd as it would to the oxide, and thus its binding energy will be less. Combining these two effects, we get an estimate of the binding energy of P in a tertiary phosphine bound to cadmium of ~ 131 eV. Thus, it is unlikely that the measured P peak corresponds to P directly datively bound to Cd.

The technique used to calculate Cd:Se ratios can also be used to determine the surface coverage of ligands on the surface of the nanocrystals by comparing the Cd and P peaks with the modification of eq 3 so that the P integral is over a spherical shell rather than over the full sphere (Figure 9). Note that, for a nanocrystal of radius 25 Å, the signal from P atoms on the surface of the nanocrystal facing the analyzer will contribute 10 times as much signal as P atoms on the surface of the nanocrystal facing away from the analyzer, so this modification is essential. Peak areas of the Cd and P peaks are then calculated and ratioed as above (Table 1). Only those samples which were dispersed in toluene are included here. Those dispersed in pyridine showed little P content. The Cd/P ratios fit best to a $1/r$ curve, indicating that the ligands are indeed on the surface. The absolute error in this measurement comes primarily from the uncertainty with which the background is fit, as in the Cd:Se ratio measurement. However, the background is modeled in the same way across all samples, so that the relative error is much smaller. Thus, trends with size are meaningful. An additional error in this measurement comes from our sample preparation. The dithiols which bind the nanocrystals to the Au surface will necessarily displace ligands from Cd surface atoms. However, we believe that this is a minor effect on our measurements of surface coverage because of the limited area of the nanocrystal surface which the dithiols are able to reach given their maximum and minimum extension. Note that this effect will cause us to slightly underestimate the total coverage on the surface and will become less significant as the nanocrystal size increases.

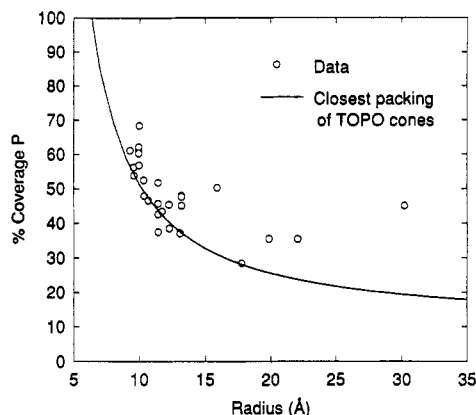


Figure 10. Percent coverage of P-containing ligands (primarily TOPO) on the cluster surface vs radius. Graph shows data as measured by XPS along with a calculation based on steric considerations (see text).

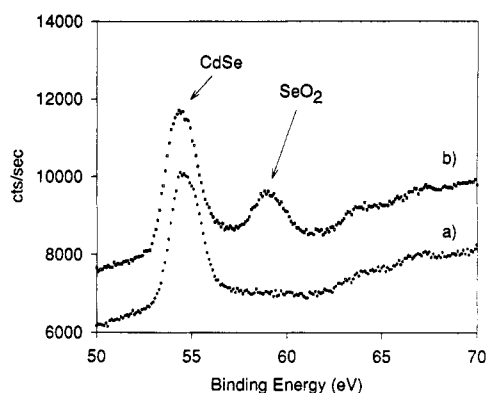


Figure 11. Oxidation of the CdSe surface-Se 3d cores: (a) 13.1-Å cluster as prepared with no air exposure; (b) 13.1-Å cluster after air exposure for 24 h.

A percent coverage of ligands on the surface was obtained by first calculating the number of CdSe units in a nanocrystal of the given radius, using the bulk density, which does not change significantly with size.²³ Then, the number of CdSe units in a nanocrystal of the given radius minus the CdSe bond length of 2.63 Å²³ was calculated, and this number was subtracted from the previous number, giving the number of Cd and Se units on the surface. Then the percent coverage is obtained by taking the P:Cd ratio and multiplying it by the total number of Cd atoms on the surface of the nanocrystal and dividing this number by the total number of Cd and Se surface atoms per nanocrystal. Thus, assuming a uniform distribution of Cd and Se on the nanocrystal surface, a 50% coverage means that every Cd atom is bound to one TOPO molecule on average, with nothing bound to the surface Se atoms. The percent coverage is larger for smaller size nanocrystals and varies from 60% to 30% (Figure 10). This is in agreement with the work of Becerra et al., which showed 55% coverage on an 18-Å-radius nanocrystal.³

Further information on the surface of nanocrystals may be obtained by studying the Cd and Se peaks over time in air. All samples developed an oxidized Se peak after spending time in air (Figure 11). The typical time for appearance of the peak was 1 day. The peak's position relative to the CdSe peak agrees with the peak position seen for Se oxides on bulk CdSe, as would be expected.²⁴ No similar oxidation of the Cd peak was observed (Figure 12a). In addition, upon oxidation of the Se, little decay in the P signal is observed (Figure 12b): over 1 week, the P signal decreased by less than 10%.

The temporal behavior of the peak is somewhat surprising. After the initial rise of the oxide peak, the peak slowly decays and then rises again (Figure 13). Oscillations continue over the period of several weeks, perhaps longer. During the time that the oxidized peak is decaying, the Cd:Se ratio is rising, indicating the loss of Se from the nanocrystal.

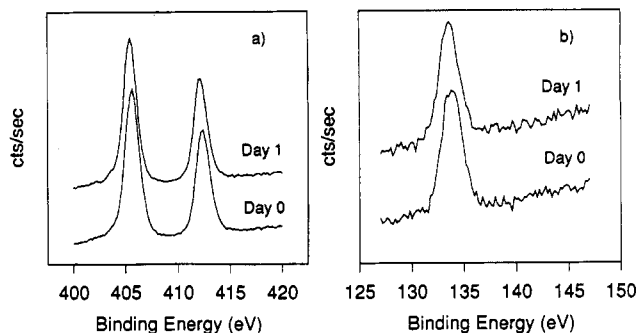


Figure 12. Cd and P cores for oxidized cluster of Figure 10: (a) Cd 3d cores; (b) P 2p cores. Note that the Cd and P cores do not change substantially.

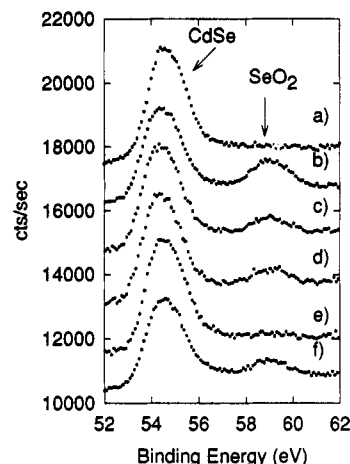


Figure 13. Oxidation of the CdSe surface-Se 3d cores: (a) 13.1-Å cluster as prepared; (b-f) cluster after 24, 48, 72, 96, and 120 h in air. Note decay of oxide peak followed by reemergence in (f).

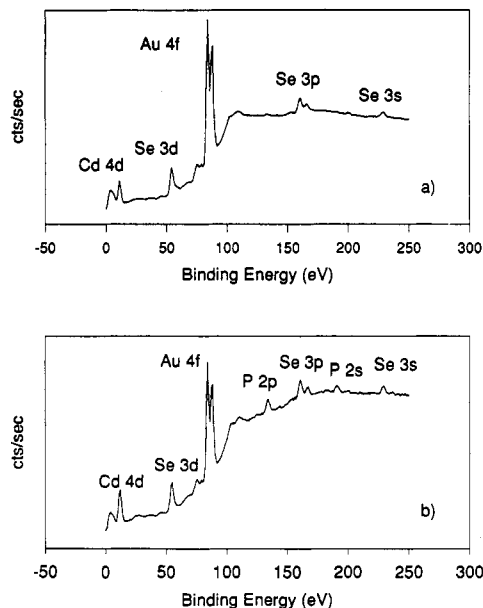


Figure 14. (a) Close-up XPS survey spectrum of CdSe clusters deposited from pyridine on gold. (b) Close-up XPS survey spectrum of CdSe clusters deposited from toluene on gold. Note the absence of P for the sample deposited from pyridine.

Surface Properties of Nanocrystals Deposited from Pyridine. Survey spectra of clusters deposited from pyridine indicate an absence of P in the spectrum (Figure 14). A close-up scan of the P region (Figure 15) reveals that a small amount of P is present. The peak shown fits to an area corresponding to a 12% coverage of the nanocrystal surface by P. Thus, while the majority of P has been removed upon dissolution in pyridine, a small amount remains on the nanocrystal surface.

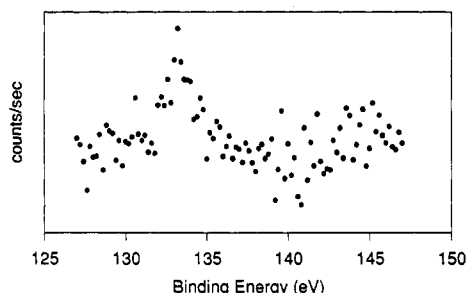


Figure 15. Close-up XPS spectrum of P 1s core region for a 14-Å CdSe nanocrystal deposited on gold from pyridine. The P signal is much lower than that shown in Figure 8. The amount of P corresponds to 12% coverage of P on the surface.

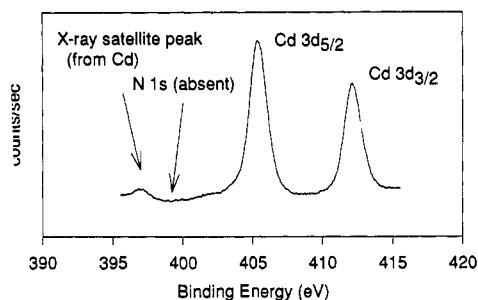


Figure 16. Close-up XPS spectrum of N 1s core region for CdSe nanocrystals deposited on gold from pyridine. Note the absence of signal from N, indicating the absence of pyridine.

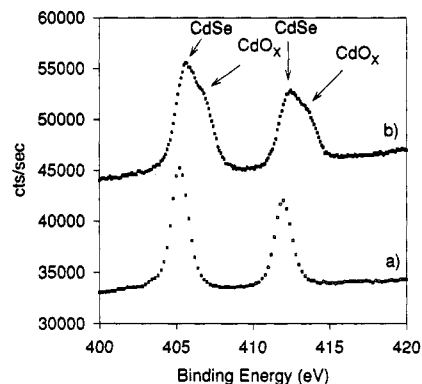


Figure 17. Oxidation of the CdSe surface—Cd 3d cores: (a) 15.9-Å cluster as prepared; (b) 15.9-Å cluster after several weeks in air.

Close-up spectra of the N 1s core region (Figure 16), which overlaps with the Cd 3d region, indicate the absence of N on the nanocrystals. Note that the small peak to lower binding energy of where the N 1s peak should be is the Cd 3d core originating from the satellite line of the Mg radiation and thus does not indicate the presence of N. The absence of both P and N indicates that pyridine displaces TOPO from the surface when the nanocrystals are dispersed. Then, when the nanocrystals are placed in vacuum the pyridine desorbs at room T, leaving behind a clean nanocrystal surface.

The oxidation of Se in the pyridine samples is similar to the oxidation in the toluene samples. However, the pyridine samples also develop an oxidized Cd peak (Figure 17). The peak appeared after the sample had been in air for several weeks. The peak's position agrees with that of oxidized Cd in bulk CdSe.

Discussion

Characteristics of Nanocrystals. CdSe nanocrystals synthesized using our methods are nearly monodisperse, much like the nanocrystals of Murray et al.⁵ However, the X-ray patterns of their nanocrystals indicate that their nanocrystals contain at least one stacking fault per crystal and are prolate, whereas the majority of our X-ray diffraction patterns are in good agreement with

spherical nanocrystals with no stacking faults.¹⁴ We believe that this difference comes about because of the higher temperature used in our synthesis. In previous work on micelle preparations of CdSe, it was shown that annealing of the nanocrystals in a high boiling point solvent, such as 4-ethylpyridine, dramatically improved the crystallinity of the nanocrystals. Subsequent work on CdS has shown that nanocrystals melt at substantially lower temperatures than the bulk material.²⁵ Thus, it is likely that crystallinity is improved by forming the nanocrystals at higher temperature. By forming the nanocrystals at temperatures ~150 °C higher than Murray et al., we do not see the stacking faults present in their nanocrystals.

Core Levels in Nanocrystals Agree with Bulk Values. As mentioned above, core level positions for Cd and Se in CdSe nanocrystals agree well with the values for bulk CdSe. This is expected, as the crystal structure is the same in the nanocrystals and in the bulk, and so little deviation in the type of bonding, and of the effect of bonding on the deeply bound core levels, should be observed.

The Nature of the Unoxidized Surface. Work on bulk CdSe has shown a strong interaction between several types of phosphines and the CdSe surface.²⁶ However, this work is based on variations in the photoluminescence of CdSe with exposure to phosphines and so does not demonstrate the nature of the binding of the phosphines to the CdSe surface.

There are two types of P compounds which could appear on the surface of our nanocrystals, based on our synthetic technique. Tributylphosphine is initially bound to Se⁰ in the stock solution. It is expected that the P–Se bond would be broken upon entrance into the hot TOPO, but the TBP could rebound to the nanocrystal surface after the crystallites have formed. In addition, the TOPO can coordinate to the surface of the nanocrystals.

Because of the P peak position, we believe that Cd–P bonds do not appear on the nanocrystal surfaces. This leaves us with the possibility of TOPO binding to either Cd or Se surface sites and of TBP binding to the surface Se sites. Because both TBP and TOPO are Lewis bases, neither of them would be likely to bind to the basic Se²⁻ on the surface. In addition, because little reduction of P signal accompanies the oxidation of the Se sites, it is clear that oxygen cannot be displacing a significant amount of P when it bonds to Se. The most it can be displacing is 10%. Finally, TOPO is known to be good at extracting Cd(II) from solution from studies on cadmium halides.²⁷ Thus, we believe that the majority of P bound to the surface is in the form of TOPO bound to Cd sites. Our FTIR measurements, which indicate the presence of complexed TOPO, also support this conclusion. It is possible that a small amount of TBP bound to Se is also present on the surface. The oxidation work and the work on samples dispersed in pyridine indicate that perhaps 10–20% of the P is bound in this way. These conclusions are further supported by the work of Becerra et al.,³ which demonstrated a total surface coverage of TOPO and TOPSe of ~55% for 18-Å nanocrystals, with 70% of this coverage due to TOPO.

The percent coverage of ligands on the nanocrystals decreases as the nanocrystal radius increases, reaching a saturation coverage of ~20%. The relative trend is in agreement with previous NMR work on surface ligand coverage of CdS nanocrystals.² One explanation for this has to do with steric considerations. On a smaller nanocrystal, the curvature is greater than for a larger nanocrystal. Because of this, the larger nanocrystals cannot accommodate as close a packing of surface ligands as the smaller nanocrystals, and so the surface coverage is lower. This can be quantified by assuming that TOPO has a roughly conical shape and calculating the number of TOPO molecules which can fit on a nanocrystal surface by taking the area of the cylinder base and dividing by the surface area of a sphere of radius $r = r_{\text{nanocrystal}} + \text{length}_{\text{TOPO}}$. Multiplying this by the closest packing fraction gives the maximum coverage possible based on the geometry of TOPO and the nanocrystals. Assuming that TOPO has a swept-out radius of 5.5 Å²⁸ and a length of 9.9 Å,²⁹ this correctly predicts

the radius dependence of the coverage in nanocrystals (Figure 10). However, in the smaller nanocrystals, the percent coverage is larger than 50%, which corresponds to more than one TOPO molecule per surface Cd atom. This can be explained by noting that we have previously determined that between 10% and 20% of the P on the surface is bound to Se. That would allow for the coverage to be between 55% and 60% in the smallest sizes, which is what we find.

The larger radius nanocrystals have somewhat larger P:Cd ratios than can be accounted for by steric considerations; i.e., the percent coverage predicted in this model is lower than is actually observed for the largest sizes. There are several ways to explain this. One is that there is excess unbound TOPO on the surface of the nanocrystals. (Note that the TOPO will not bind by itself to the Au surfaces, and so excess TOPO not attached to nanocrystals cannot be a factor.) This is unlikely because of the substantial amount of rinsing done on the nanocrystals. Any TOPO not bound should have been removed in this process. The absence of the bulk TOPO-P-O peak in IR confirms this. Another possibility is the presence of small nanocrystals within the distribution of the larger nanocrystals. Small nanocrystals would artificially raise the coverage of the larger nanocrystals, and their presence would be obscured in the optical absorption spectrum. They should be observed in TEM, and we have not seen sufficient numbers to justify this conclusion. A further explanation is that the higher saturation coverage results from the presence of TBP in place of TOPO on the surface. This would also allow closer packing of P ligands than predicted by pure TOPO packing and thus would increase the saturation coverage. This would increase the allowed coverage, but not by the amount necessary for several of the larger samples. Finally, the model's assumption of a homogeneous, spherical surface may be incorrect in the larger sizes. Increased surface inhomogeneity would account for a greater number of possible sites in the larger nanocrystals and hence allow for the larger number of TOPO molecules on the surface than predicted. For example, as larger regions of surface develop on nanocrystals, facets could develop. The resulting faces would more readily support a well-ordered interpenetration of the octane chains than would a spherical surface, because of the larger length scale over which the chains would have to order. This argument does not imply that larger nanocrystals would have higher percent coverage than smaller nanocrystals, only that larger nanocrystals would have higher percent coverages than is predicted by the closest packing of noninterpenetrating cones, which is what we have calculated.

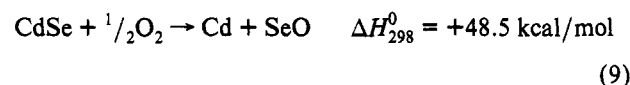
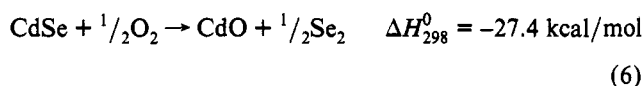
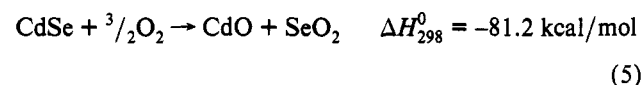
Thus, XPS indicates that the nanocrystals as prepared have a surface which consists of predominantly unbonded Se atoms and bonded Cd atoms, with no more than 20% of the P ligands on the surface bound to Se. The Cd atoms are bonded to TOPO to the extent that it is sterically allowed. However, the saturation coverage is higher than that reached by assumption of only TOPO on the surface, which can be explained by two effects: the presence of small amounts of TBP on the surface, in addition to TOPO, allowing for closer packing, and the presence of facets on the larger nanocrystals.

Oxidation of the Nanocrystals Deposited from Toluene. Several studies have been done on the oxidation of bulk CdS,³⁰ CdSe,³¹ and CdTe³² surfaces using primarily XPS, Auger, and resistance/conductance measurements. Some common conclusions have emerged from these studies. Upon the introduction of a clean CdE (E = S, Se, Te) surface into air, a monolayer of oxygen physisorbs onto the surface. The sticking coefficient is 10^{-13} – 10^{-14} for perfect surfaces,^{31a} so at atmospheric pressure a perfect surface would adsorb a monolayer in ~ 4 h. This adsorption will be much quicker for a rougher surface, as would be present for the nanocrystals, as evidenced by the saturation time in conductance studies, which can be minutes at room temperature for real (imperfect) surfaces.

Based on conductivity studies, the oxygen is adsorbed via a transfer of electron density from the semiconductor to the oxygen.

The oxygen then proceeds to break the chalcogen back bonds to the bulk semiconductor. At this point some type of surface oxide is formed. However, the exact nature of the oxide formed is not clear. Most XPS studies show the existence of oxidized chalcogen. The oxide is most likely chemisorbed at this point, but it is also possible that the oxide formed is only physisorbed to the bulk. The Cd 3d peak positions for CdE, CdEO₃, and CdO are very close to each other, and most researchers argue that the only way to tell the difference between these species is in the Cd Auger peak. However, the differences there are also small, making it difficult to reach conclusions about the nature of the oxide.

Thermodynamic considerations point to the compound oxide as the most probable candidate upon seeing an oxidized Se peak, followed by SeO₂.³³



In our system, the majority of Cd surface atoms are bonded to the TOPO ligand, making the formation of the compound oxide unlikely. Thus, it is most likely that the oxide we see is SeO₂. In addition, because of the oxide peak position, which corresponds to the peak position for bulk SeO₂, it seems likely that we are forming SeO₂ in a separate phase from the nanocrystal, by process 7. In addition, experiments on CdS and CdTe nanocrystals in solution³⁴ have demonstrated the formation of sulfates and tellurates in solution upon exposure of the solutions to oxygen and light, supporting the creation of an oxide out of solution.

Our data are in good agreement with the bulk data. Although we cannot confirm this with XPS, it is likely that immediately upon exposure to air, oxygen physisorbs onto the CdSe surface. In TOPO-capped nanocrystals, this would proceed with electron density from the surface Se²⁻ being transferred to adsorbing oxygen. Over time, SeO₂ develops, as evidenced by XPS. However, the presence of the SeO₂ peak in the XPS indicates that the Se in SeO₂ is no longer bound to the nanocrystal surface. Thus, over time the SeO₂ on the surface desorbs, based on purely thermodynamic arguments of partial pressure. This will be followed by the same cycle of physisorption and chemisorption on the remaining or freshly exposed Se. Over time, this will cause the surface to be depleted of Se, as evidenced by the increase of the Cd:Se ratio upon oxidation.

Surface Properties of Nanocrystals Deposited from Pyridine. In nanocrystals in which the TOPO surface groups have been displaced by pyridine in solution, the nanocrystals have no ligand attached to their surface once taken out of solution and bound to gold. At most, 10–15% of their surface is covered, based on XPS measurements. Thus, oxygen can easily adsorb onto both Cd and Se sites and eventually bond with both, as in the bulk. It is interesting to note that the peak position for bulk CdO is actually at lower binding energy than CdSe.³⁵ However, in our experiment and in an experiment on bulk CdSe in which films were heated in air,²⁴ the oxide peak of Cd is shifted to higher energy. This is in better agreement with a compound oxide than with CdO, so it may be that in this case CdSeO₃ is being formed,

rather than CdO and SeO₂, as would be predicted based on thermodynamic arguments (eq 4).

Conclusion

In conclusion, we have measured XPS spectra on a variety of sizes of CdSe nanocrystals covalently bound to gold surfaces. We have seen that the core levels obtained in this way are in agreement with bulk values for CdSe. In addition, we have used XPS to probe the surface of CdSe nanocrystals and have determined that the Cd surface sites are passivated by TOPO and that Se surface sites are predominantly unbonded, in agreement with a recent NMR study.³ When stored in air, Se surface sites are oxidized, forming an SeO₂ surface film which is physisorbed to the nanocrystal surface and which degrades over time. In nanocrystals deposited from pyridine, neither the Cd or Se surface sites are completely passivated. When these are stored in air, both Cd and Se surface sites oxidize. XPS techniques can be readily extended to a variety of soluble semiconductor systems and provide a versatile way to measure the surface composition of semiconductor nanocrystals.

Acknowledgment. J.E.B.K. thanks C. B. Murray for helpful discussion regarding the surface of CdSe nanocrystals. Thanks to R. K. Grubbs and J. J. Shiang for assistance with Raman spectroscopy and to A. V. Kadavanich for the TEM. Thanks to the M. Majda group for the use of their evaporator. Thanks to Dr. Kin-Man Yu of LBL for his work on RBS. We thank the National Center for Electron Microscopy at Lawrence Berkeley Laboratory for the use of the electron microscope. J.E.B.K. acknowledges a fellowship from the National Science Foundation. A.P.A. acknowledges a fellowship from the Alfred P. Sloan Foundation. This work was supported by the Department of Energy under contract DE-AC0376SF00098.

References and Notes

- Hoener, C. F.; Allan, K. A.; Bard, A. J.; Campion, A.; Fox, M. A.; Mallouk, T. E.; Webber, S. E.; White, J. M. *J. Phys. Chem.* **1992**, *96*, 3812.
- Sachleben, J. R.; Wooten, E. W.; Emsley, L.; Pines, A.; Colvin, V. L.; Alivisatos, A. P. *Chem. Phys. Lett.* **1992**, *198*, 431.
- Becerra, L.; Murray, C. B.; Griffin, R. G.; Bawendi, M. G. *J. Chem. Phys.*, in press.
- Colvin, V. L.; Goldstein, A. N.; Alivisatos, A. P. *J. Am. Chem. Soc.* **1992**, *114*, 5221.
- Murray, C. B.; Norris, D. B.; Bawendi, M. G. *J. Am. Chem. Soc.* **1993**, *115*, 8706.
- Klug, H. P.; Alexander, L. E. *X-ray Diffraction Procedures for Polycrystalline and Amorphous Materials*, 1st ed.; John Wiley & Sons: New York, 1974; Chapter 9.
- Goldstein, A. N.; Tu, A.; Alivisatos, A. P. Size Distributions of CdSe Nanocrystals. To be submitted for publication.
- Porter, M. D.; Bright, T. B.; Allara, P. L.; Chidsey, C. E. D. *J. Am. Chem. Soc.* **1987**, *109*, 3559.
- Wasserman, S. R.; Biebuyck, H.; Whitesides, G. M. *J. Mater. Res.* **1989**, *886*.
- Calvert, J. M.; Georger, J. H.; Peckerar, M. C.; Pehrsson, P. E.; Schnur, J. M.; Schoen, P. E. *Thin Solid Films* **1992**, *210*, 359.
- Goss, C. A.; Charych, D. H.; Majda, M. *Anal. Chem.* **1991**, *63*, 85.
- Shiang, J. J.; Risbud, S. H.; Alivisatos, A. P. *J. Chem. Phys.* **1993**, *98*, 8432.
- Pancove, J. I. *Optical Processes in Semiconductors*, 1st ed.; Dover Publications: New York, 1975; Appendix.
- Tolbert, S. H.; Alivisatos, A. P. Size Dependence of a First Order Solid-Solid Phase Transition: The Wurtzite to Rocksalt Transformation in CdSe Nanocrystals. To be submitted for publication in *J. Chem. Phys.*
- Cotton, F. A.; Barnes, R. D.; Bannister, E. J. *Chem. Soc.* **1960**, 2199.
- Shiang, J. J.; Grubbs, R. K.; Katari, J. E. B.; Alivisatos, A. P. Resonance Raman Spectroscopy of CdSe Nanocrystals. To be submitted for publication in *J. Chem. Phys.*
- Wagner, C. D.; Riggs, W. M.; Davis, L. E.; Moulder, J. F.; Muilenberg, G. E. *Handbook of X-ray Photoelectron Spectroscopy*; Perkin-Elmer: Eden Prairie, MN, 1978.
- The values of *S* used for this study are taken from the manual accompanying the PHI 5300 spectrometer and are specifically measured for the PHI 5300 with the appropriate lenses.
- Cardona, M.; Ley, L., Eds. *Photoemission in Solids*; Springer-Verlag: New York, 1978; Vol. 1, Chapter 1.
- Vesely, C. J.; Langer, D. W. *Phys. Rev. B* **1971**, *4*, 451.
- Colvin, V. L.; Alivisatos, A. P.; Tobin, J. G. *Phys. Rev. Lett.* **1991**, *66*, 2786.
- Peakfit version 3.10; Jandel Scientific, 1992.
- Marcus, M. A.; Flood, W.; Steigerwald, M. L.; Brus, L. E.; Bawendi, M. G. *J. Phys. Chem.* **1991**, *95*, 1572.
- Sebastian, P. J.; Sivaramakrishnan, V. *Vacuum* **1990**, *41*, 647.
- Goldstein, A. G.; Echer, C. M.; Alivisatos, A. P. *Science* **1992**, *256*, 1425.
- (a) Murphy, C. J.; Ellis, A. B. *Polyhedron* **1990**, *9*, 1913. (b) Murphy, C. J. *J. Electrochem. Soc.* **1990**, *137*, 220C.
- Sato, K.; Takahashi, Y.; Suzuki, T.; Sawada, K. *J. Chem. Soc., Dalton Trans.* **1989**, 1259.
- Pappa-Louisi, A.; Nikitas, P.; Jannakoudakis, D. *Electrochim. Acta* **1984**, *29*, 515.
- (a) Norman, N.; Mathisen, H. *Acta Chem. Scand.* **1961**, *15*, 1747. (b) Rose, J. P.; Lalancette, R. A.; Potenza, J. A.; Schugar, H. J. *Acta Crystallogr. B* **1980**, *36*, 2409.
- (30) Auger and XPS Studies: (a) Amalnerkar, D. P.; Sainkar, S. R.; Badrinarayanan, S. *J. Mater. Sci. Lett.* **1989**, *8*, 862. (b) Lagowski, J.; Lichtensteiger, M.; Williams, P. M. *Surf. Sci. Lett.* **1979**, *84*, L223. (c) Lichtensteiger, M.; Webb, C.; Lagowski, J. *Surf. Sci.* **1980**, *97*, L375. (d) Marychurch, M.; Morris, G. C. *Surf. Sci.* **1985**, *154*, L251. Resistance and capacitance studies: (e) Bhide, V. G.; Jatar, S.; Rastogi, A. C. *Pramana* **1977**, *9*, 399. (f) Legre, J. P.; Martinuzzi, S. *Phys. Status Solidi A* **1970**, *1*, 689. (g) Weitzel, C. E.; Monteith, L. K. *Surf. Sci.* **1973**, *40*, 555. (h) Mark, P. J. *Phys. Chem. Solids* **1965**, *26*, 959.
- (31) Auger and XPS Studies: (a) Brillson, L. J. *Surf. Sci.* **1977**, *69*, 62. (b) Ebina, A.; Asano, K.; Suda, Y.; Takahashi, T. *J. Vac. Sci. Technol.* **1980**, *17*, 1074. (c) Ebina, A.; Asano, K.; Takahashi, T. *Phys. Rev. B* **1980**, *22*, 1980. (d) Sebastian, P. J.; Sivaramakrishnan, V. *Vacuum* **1990**, *41*, 647. Conductivity and resistance: (e) Allongue, P.; Tenne, R. J. *Electrochem. Soc.* **1991**, *138*, 261. (f) Bube, R. H. *J. Electrochem. Soc.* **1966**, *113*, 795. (g) Chan, D. S. H.; Hill, A. E. *Thin Solid Films* **1976**, *38*, 163. (h) Sebastian, P. J.; Sivaramakrishnan, V. *J. Appl. Phys.* **1989**, *65*, 237. (i) Somorjai, G. A. *J. Phys. Chem. Solids* **1963**, *24*, 175. (j) Wagner, R. G.; Breitweiser, G. C. *Solid-State Electron.* **1969**, *12*, 229.
- (32) XPS and Auger Studies: (a) Choi, S. S.; Lucovsky, G. J. *Vac. Sci. Technol. B* **1988**, *6*, 1198. (b) Chu, T. L.; Chu, S. S.; Ang, S. T. *J. Appl. Phys.* **1985**, *58*, 3206. (c) Davis, G. D.; Sun, T. S.; Buchner, S. P.; Byer, N. E. *J. Vac. Sci. Technol.* **1981**, *19*, 472. (d) Gaugash, P.; Milnes, A. G. *J. Electrochem. Soc.* **1981**, *128*, 924. (e) Häring, J.-P.; Werthen, J. G.; Bube, R. H.; Gulbrandsen, L.; Jansen, W.; Luscher, P. J. *Vac. Sci. Technol. A* **1983**, *1*, 1469. (f) Humphreys, T. P.; Patterson, M. H.; Williams, R. H. *J. Vac. Sci. Technol.* **1980**, *17*, 886. (g) Kohiki, S.; Nishikura, K.; Wada, T.; Hirao, T. *Appl. Surf. Sci.* **1992**, *59*, 39. (h) Morgen, P.; Silberman, J. A.; Lindau, I.; Spicer, W. E.; Wilson, J. A. *J. Electron. Mater.* **1982**, *11*, 597. (i) Rhiger, D. R.; Kvaas, R. E. *J. Vac. Sci. Technol.* **1982**, *21*, 168. (j) Ricco, A. J.; White, H. S.; Wrighton, M. S. *J. Vac. Sci. Technol. A* **1984**, *2*, 910. (k) Silberman, J. A.; Laser, D.; Lindau, I.; Spicer, W. E.; Wilson, J. A. *J. Vac. Sci. Technol. B* **1984**, *2*, 589. (l) Solzbach, U.; Richter, H. J. *Surf. Sci.* **1980**, *97*, 191. (m) Tanaka, S.; Bruce, J. A.; Wrighton, M. S. *J. Phys. Chem.* **1981**, *85*, 3778. (n) Varma, R. R.; Patterson, M. H.; Williams, R. H. *J. Phys. D* **1979**, *12*, L71. (o) White, H. S.; Ricco, A. J.; Wrighton, M. S. *J. Phys. Chem.* **1983**, *87*, 5140. (p) Wu, Y. S.; Becker, C. R.; Waag, A.; Schmiedl, R.; Einfeldt, S.; Landwehr, G. *J. Appl. Phys.* **1993**, *73*, 7385. (q) Yi, X.; Liu, Q.; Zhao, X.; Wong, G. K. *J. Phys. D* **1990**, *23*, 912. Other techniques: (r) Aspnes, D. E.; Arwin, H. *J. Vac. Sci. Technol. A* **1984**, *2*, 1309. (s) Courreges, F. G.; Fahrenbruch, A. L.; Bube, R. H. *J. Appl. Phys.* **1980**, *51*, 2175. (t) Hage-Ali, M.; Stuck, R.; Saxena, A. N.; Siffert, P. *Appl. Phys.* **1979**, *19*, 25. (u) Ponce, F. A.; Sinclair, R.; Bube, R. H. *Appl. Phys. Lett.* **1981**, *39*, 951. (33) Kubaschewski, O.; Alcock, E. B. *Metallurgical Thermochemistry*, 5th ed.; Pergamon Press: Oxford, 1979; p 267ff. (34) (a) Henglein, A. *Top. Curr. Chem.* **1988**, *143*, 113. (b) Fischer, C. H.; Henglein, A. *J. Phys. Chem.* **1989**, *93*, 5578. (35) Gaarenstroom, S. W.; Winograd, N. *J. Chem. Phys.* **1977**, *67*, 3500.